



Title	The role of saltwater and waves in continental shelf formation with seaward migrating clinoform
Author(s)	Iwasaki, Toshiki; Parker, Gary
Citation	Proceedings of the National Academy of Sciences of the United States of America (PNAS), 117(3), 1266-1273 https://doi.org/10.1073/pnas.1909572117
Issue Date	2020-01-21
Doc URL	http://hdl.handle.net/2115/78943
Type	article (author version)
File Information	Iwasaki_Parker_PNAS_Accepted.pdf



[Instructions for use](#)

1 **Title: The role of saltwater and waves in continental shelf formation:**
2 **seaward-migrating clinoform**

3

4 **Short title: Role of saltwater and waves in continental shelf formation**

5

6 Major category: Physical sciences

7 Minor category: Earth, Atmospheric, and Planetary Sciences

8

9 **Toshiki IWASAKI¹⁾ and Gary PARKER²⁾**

10 1) Graduate school of Engineering, Hokkaido University, Sapporo, Japan

11 ORCID ID: 0000-0002-7196-3619

12 2) Department of Civil and Environmental Engineering and Department of Geology,

13 University of Illinois Urbana-Champaign, Urbana, IL, USA

14 ORCID ID: 0000-0001-5973-5296

15 Competing interest statement: G.P. and Hajime Naruse are co-authors on a 2016 research article in

16 Sedimentology.

17 Corresponding author: Gary Parker (parkerg@illinois.edu)

18

19 **Abstract:**

20 Continental shelves have generally been interpreted as drowned coastal plains
21 associated with the allogenic effect of sea level variation. Here, without disputing this
22 mechanism we describe an alternative autogenic mechanism for subaqueous shelf
23 formation, driven by the presence of dissolved salt in seawater and surface waves.
24 We use a numerical model describing flow hydrodynamics, sediment transport and
25 morphodynamics in order to do this. More specifically, we focus on two major
26 aspects; 1) the role of saltwater in the subaqueous construction of continental
27 shelves, and 2) the transformation of these shelves into seaward-migrating clinofolds
28 under the condition of repeated pulses of water and sediment input and steady wave
29 effects, but no allogenic forcing such as sea level change. In the case for which the
30 receiving basin contains fresh water of the same density as the sediment-laden river
31 water, the hyperpycnal river water plunges to form a turbidity current that can run
32 out to deep water. In the case for which the receiving basin contains sea water but
33 the river contains sediment-laden fresh water, the hypopycnal river water forms a
34 surface plume that deposits sediment proximally. This proximate proto-shelf can then
35 grow to wave base, after which wave-supported turbidity currents can extend it
36 seaward. The feature we refer is synonymous with near-shore mud belts.

37

38 **Key words:** continental shelves, dissolved salt, wave base, hypopycnal flows, mud
39 belts

40

41 **Significance statement:**

42 Continental shelves have been generally interpreted to be coastal plains that have
43 been drowned by sea level rise. Here we offer an alternative mechanism. Dissolved
44 salt in seawater generally forces sediment-laden freshwater from rivers into surface
45 water flows, from which sediment (mud) settles out in the near-shore zone. Over
46 time, this platform can build up to wave base, constructing a shelf within a mud belt.
47 Wave-induced sediment resuspension can drive the seaward extension of the shelf.
48 This implies that changing sea level is not the only mechanism for building
49 continental shelves.

50 /body

51

52 **Introduction**

53 Continental shelves are located at the buffer zone between the terrestrial and deep
54 ocean environments. The morphology and morphodynamics of continental shelves
55 has received significant attention in the fields of geology, engineering, and
56 environmental science [e.g., 1-4]. However, the formational processes of continental
57 shelves remain incompletely understood, in part because of the long-term geological
58 processes associated with their formation and maintenance.

59 An important characteristic of continental shelves is their relatively shallow
60 water depth (up to ~120 m at the shelf-slope break) [3]. Although this depth varies
61 [5], it implies the presence of a dominant controlling factor determining both water
62 depth and continental shelf formation. A common hypothesis is that continental
63 shelves are drowned ancient coastal plains that formed during lowstands [3, 6, 7].
64 This general hypothesis implies that the shelf surface originally developed via
65 long-term subaerial processes at lowstand, before being submerged by later sea level
66 rise. According to this mechanism, the sediment on continental shelves is relict. This
67 model gives a reasonable description of many shelves, such as that of the East Coast
68 of the United States [e.g., 6, 8]. However, recent extensive investigations of
69 continental shelves [e.g., 9] and proto-shelves [e.g., 10, 11] using stratigraphic
70 measurements, isotopic analysis of deposited sediment, and drill-core samples imply

71 that, even under the present high stand, shelves and proto-shelves can form and
72 extend purely by a combination of subaqueous hydrodynamics, sediment transport,
73 and morphodynamic processes. These shelves are typically characterized as mud
74 belts or mud wedges (e.g. the Amazon mud belt [12], the northern Gulf of Mexico
75 mud belt [11], and the Yellow Sea mud wedge [13]. Gao and Collins [14] report
76 Holocene shelf mud deposits of up to 50 m in thickness. Indeed, much of the Italian
77 Adriatic shelf clinoform was emplaced in the late Holocene under stillstand conditions
78 (e.g., [15], Figure 3 of Maselli et al. [16]).

79 Steckler et al. [17] reconstructed the development of the New Jersey
80 continental shelf based on seismic analysis and sequence stratigraphy, and showed
81 clear clinoform migration and subsequent development of a continental shelf at long
82 geological time scale. They also estimated paleo-water depths on the continental
83 shelf, indicating that the clinoform rollover along the New Jersey continental margin
84 has been submerged regardless of sea level. This suggests that the sea level
85 difference between high stand and low stand cannot universally explain the
86 hypothesis of continental shelves as being ancient coastal plains. Subaqueous
87 processes (e.g., sediment supply [2], wave-, tide-, and wind-driven currents [18], and
88 sediment re-distribution by turbidity currents [19, 20]) may also play important roles
89 in the morphodynamics of continental shelves. In addition to sequence stratigraphy

90 [21], process-based approaches incorporating the concepts of morphodynamics or
91 stratodynamics [e.g., 22] are crucial for a better understanding of the genesis of
92 continental shelves.

93 Here, we present a formational mechanism for continental shelves that
94 involves multiple interactions among terrigenous sediment supply, wave-current
95 hydrodynamics, subaqueous sediment transport, and subsequent morphodynamic
96 processes. The focus of this study concerns sedimentary continental shelves that have
97 sediment deposition as the main formative driver (e.g., Cenozoic New Jersey passive
98 margin [17]), rather than structural shelves, whose formation is determined by
99 tectonic process (e.g., Quaternary active transform margin, central California [8]), or
100 shelves governed by processes involving ice. More specifically, we demonstrate 1) the
101 crucial role played by salt dissolved in ocean water in the formation of continental
102 shelves, and 2) the long-term development of shelf morphology due to
103 seaward-migrating clinoforms. Both these elements are intimately associated with
104 interactions between fluvial suspended sediment supply, sediment deposition from
105 hypopycnal plumes, and wave-induced sediment re-distribution on the shelf.

106 The transport characteristics of suspended load and/or mud supplied from
107 rivers into a coastal ocean are key to understanding where sediment is deposited on
108 the sea floor, and how sediment transport creates seascapes. Apart from rivers

109 carrying unusually high sediment loads [23, 24], sediment-laden fresh river water is
110 generally lighter than ambient salt water, preventing direct plunging of river water
111 onto the sea bed. Instead, this density barrier results in the formation of a surface
112 plume (hypopycnal flow) rather than a bottom current (hyperpycnal flow) [e.g., 25].
113 In this configuration, settling of fluvial sediment from plumes, and the subsequent
114 development of weak turbidity currents may play dominant roles in the supply of
115 river-derived sediment to continental shelves [e.g., 26, 27]. The differences in the way
116 that hypo- and hyperpycnal flows move sediment and create morphology are
117 significant; however, the effects of these different flow regimes on shelf morphology
118 have not yet been clearly demonstrated.

119 We here consider a fresh water lake as a counterpoint to the ocean
120 environment to illustrate the effects of hypo- and hyperpycnal flows on the
121 morphodynamics of shelf-like morphology. Because sediment supply from rivers is
122 thought to be a main driver of continental shelf formation [2], similar shelf
123 morphology might be expected in ancient terrestrial lakes which have substantial
124 fluvial sediment supply. However, shelf morphology in the form of a bench that
125 connects delta to delta is rarely seen in lacustrine environments [e.g., 28, 29]. We
126 hypothesize that this is due to the different hydrodynamics and sediment transport
127 between the two environments associated with dissolved salt in ambient water.

128 Another focus of this research is to understand wave effects on the
129 resuspension and redistribution of deposited sediment on the shelf, and the resulting
130 shelf morphodynamics. Surface waves induced by storms, for example, cause
131 movement of the water body only to a specified depth below the water surface (wave
132 base). When sea floor elevation exceeds wave base, surface waves can generate a
133 wave-induced bottom boundary layer, resulting in resuspension of deposited
134 sediment and subsequent truncation of the shelf surface. Wave-base theory offers
135 another powerful element for explaining the evolution of continental shelves [e.g.,
136 30-33]. This hypothesis has, however, only limited implications for continental shelf
137 genesis, in that it acts only when the shelf is above wave base. Wave base changes as
138 sea level varies, so an extremely long period of constant sea level is required to
139 truncate the entire surface of a shelf. The duration of the present sea level from the
140 end of the last glaciation may not be sufficient for this [34]. Dietz and Menard [35]
141 note that wave base is typically not deep enough to explain the sustained water
142 depth on continental shelves. However, waves do play an important role in sediment
143 redistribution on the shelf, and contribute to clinoform development even during the
144 present-day highstand [e.g., 19, 20, 36]. This indicates that the wave effect is a key
145 factor explaining continental shelf formation, which is attributed to
146 seaward-migrating clinoforms.

147 In this study, we use a numerical model to investigate the formative
148 mechanisms of continental shelves. The goal is to investigate the interaction between
149 sediment dispersal due to hypopycnal flow, surface wave effects on the redistribution
150 of deposited sediment on the continental margin, and shelf morphodynamics in
151 terms of migrating clinoforms. The individual effects of each process on margin
152 development have been studied through field observations, laboratory experiments,
153 numerical modeling, and theoretical analysis [e.g., 11, 37-39]. However, because of
154 the complexity of the system, the role of multiple interacting mechanisms on
155 continental margin development remains under-investigated. The numerical model
156 and calculational conditions are considerably simplified in this study (for example,
157 alongshore processes are not included, *Methods*), but it still captures the essential
158 complexities of the system suggested by previous studies. Our study provides the first
159 description of autogenic continental shelf formation due to subaqueous
160 hydrodynamics and sediment transport, in the absence of allogenic effects such as
161 sea-level variation, tectonism, and changes in sediment supply rate.

162

163 **Results**

164 **Morphodynamic differences between hypopycnal and hyperpycnal flows**

165 The aim of our first numerical simulation is to determine the differences in shelf

166 morphodynamic processes associated with hypo- and hyperpycnal flows. The initial
167 bed geometry for this calculation represents an idealized, small continental margin of
168 length 15 m, consisting of a low shelf, slope, and rise (see *SI Appendix, Fig.S1*). We
169 imposed a fresh, sediment-laden water supply of constant water discharge and
170 suspended sediment concentration from an upstream inlet surface layer. The key
171 factor differentiating the two flow regimes in the simulations is the dissolved salt in
172 the ambient water. To simulate a hypopycnal flow, we set the excess density of the
173 ambient water due to dissolved salt at 40 kg/m^3 , (so that the receiving basin mimics
174 the ocean). This ambient water has a density that is larger than the excess density of
175 the inflow water carrying suspended sediment. For the hyperpycnal flow cases, the
176 excess density of the ambient water due to salt is set to be zero (i.e., the receiving
177 basin mimics a freshwater lake), resulting in the direct plunging of the
178 sediment-laden inflow water. This computational setting highlights the role of
179 saltwater in the flow regime and subsequent shelf morphodynamics. Other
180 calculation conditions and detailed computational settings are in *SI Appendix,*
181 *Methods and Results*. We performed several numerical simulations by changing
182 parameters (e.g., water discharge, sediment concentration etc.) for sensitivity
183 analysis, but below we show the results of a typical case (Case 1 in *SI Appendix,*
184 *Table-S1*).

185 Figures 1 and 2 show the simulation results for flow and sediment transport
186 behavior generated by a hypopycnal flow (Figure 1) and a hyperpycnal flow (Figure 2)
187 respectively. For the hyperpycnal flow, the inflowing sediment-laden fresh water
188 immediately plunges to the bottom, generating a turbidity current (Fig. 2a-1). This
189 flow efficiently delivers sediment to the rise region (Fig. 2a-3). Flow and sediment
190 transport processes associated with hypopycnal flow are, however, quite different.
191 The initial density relationship between the inflow and the ambient water satisfies a
192 stable stratification condition in terms of total density, generating a positively
193 buoyant, hypopycnal plume (Fig. 1a-1). The fresh water flows near the surface and
194 eventually reaches the downstream end of the domain (Fig. 1b-3); however,
195 suspended sediment does not follow this behavior. As shown in Fig. 1a-2, plumes
196 develop underneath the surface plume, aiding removal of sediment from the surface
197 plume. Because sediment has a finite settling velocity, the transport process differs
198 between dissolved salt and suspended sediment. As sediment settles out it creates a
199 heavy layer below the body of the plume (“nose region”, [40, 41]). Here the sediment
200 of the surface plume mixes with ambient salt water just below the surface plume.
201 This layer is unstable in terms of total density because the sediment settles into saline
202 water, being heavier than the saline water below or the fresh water above. This
203 results in a Rayleigh-Taylor-type instability. This settling-driven convection generates a

204 downward flow to the bed, removing sediment from the plume much faster than the
205 settling velocity of individual sediment particles (scavenging [42]). Because of this
206 sediment loss, the surface plume is free of suspended sediment near the downstream
207 end (Fig. 1a-3). Instead, sediment removed from the hypopycnal plume generates a
208 secondary hyperpycnal plume on the slope (Fig. 1a-3). These processes, namely,
209 settling-driven convection occurring underneath a hypopycnal plume and subsequent
210 formation of a secondary turbidity current, are also observed in some experimental
211 studies [39, 43]. A comparison of the velocity fields between the two flow regimes
212 (Figs. 1-3b and 2-3b) indicates that this secondary turbidity current is not as strong as
213 the primary turbidity current of the hyperpycnal case. Sediment transport into the
214 rise region due to this weak turbidity current is less intense than the hyperpycnal case.
215 In addition, the potential for re-entrainment of sediment on the shelf is small in the
216 hypopycnal case, which instead contributes to sediment deposition on the shelf and
217 slope. This may indicate that the sediment mixing and turbidity current generated by
218 hypopycnal flows have important roles in proximal sedimentation, but only limited
219 effects on the flow and morphodynamics in the deep ocean. We illustrate below that
220 this tendency to capture sediment proximally is one of the fundamental building
221 blocks of continental shelves.

222 The hydrodynamics and sediment transport dynamics of hypo- and

223 hyperpycnal flows result in different morphodynamic behavior of the shelf. Figure 3
224 shows the bed surface profiles obtained by hypo- and hyperpycnal flows in this case
225 after 4 hours (4 one-hour events) of simulation. It shows that 1) hypopycnal flow
226 contributes more proximal sediment deposition on the shelf than hyperpycnal flow,
227 and 2) conversely, hyperpycnal flow transports more sediment onto the rise region
228 than hypopycnal flow. In this simulation, the initial geometry of the shelf is horizontal
229 for simplicity, so the depositional features of hyperpycnal flow are over-emphasized
230 on the shelf region. Even so, the hyperpycnal flow cannot induce nearly as much
231 sediment deposition on the shelf as the hypopycnal flow. The numerical results
232 regarding sensitivity of modelled morphodynamics of the shelf show that this trend is
233 universal to all the cases we tested (*SI Appendix, Results*).

234 These results show that, at least in our simplified model, hypopycnal flow
235 contributes primarily to proximal deposition of supplied fluvial sediment on the shelf,
236 whereas hyperpycnal flow predominantly carries sediment to the deep ocean. These
237 features indicate that dissolved salt in the ambient water has an important role in
238 controlling the fate and transport of sediment on the shelf, and thus shelf formation.
239 However, the results also imply that hypopycnal flows themselves rarely induce
240 erosion of deposited sediment on the shelf. If we were to continue the simulation for
241 a sufficiently long time, the shelf region would eventually be filled with sediment, and

242 be converted to coastal plain. Channelization cannot be captured in this 2D model but
243 could be if extended to 3D [44]. There thus needs to be a factor that limits deposition
244 on the shelf. We identify this factor as wave action. As hypopycnal flows build up the
245 shelf, the shelf surface eventually reaches wave base. Wave action can then create
246 weak wave-supported turbidity currents that deliver sediment from the shelf to the
247 rise, i.e., below wave base. This would allow for a near-bypass condition on the shelf,
248 with a migrating clinoform at its outer edge.

249

250 **Wave effects on the development of seaward-migrating clinoforms**

251 Here, we focus on the case of hypopycnal flow in order to focus on continental shelf
252 formation. This is because hyperpycnal flows contribute less to proximal sediment
253 deposition on the shelf surface; this deposition is likely a key factor governing shelf
254 extension. The computational conditions of this run are essentially the same as the
255 calculation shown above, but some changes are made as follows. First, we extend the
256 continental domain length from 15 m to 30 m (so the computational domain is 30 m
257 long, but the computational grid size is maintained) and remove the initial shelf from
258 the computational domain. This change allows a large accommodation space for
259 sediment deposition, and shows whether the model itself generates shelf formation
260 and development. Second, we include wave effects on sediment transport

261 (specifically, sediment entrainment from the bed) based on linear wave theory (*SI*
262 *Appendix, Methods, Eqs. (S14)-(S19)*). The important parameters of this model are
263 the significant wave height (H_s) and the wave period (T_w). We set these as $H_s = 0.05$
264 m and $T_w = 1$ s, respectively. These values are quite large for our small,
265 laboratory-scale flume, but the erosional force of waves associated with these
266 parameters will indeed be shown to be balanced by the sediment supply rate onto
267 the shelf. Third, the upstream boundary condition is changed to repeated pulse
268 inputs instead of a steady discharge condition, so as to simulate river floods. One
269 repeated cycle consists of two time periods: steady water supply with constant
270 sediment concentration for a specified period (T_{flood}), and no water or sediment
271 supply for another specified period (T_{wave}). Sediment supply (the depositional driver)
272 occurs only in period T_{flood} , while the wave effect (the erosional driver) is
273 superimposed throughout the entire calculation. In this computational setting, T_{flood}
274 characterizes sediment supply during a flood event into the ocean, whereas T_{wave}
275 characterizes resuspension of deposited sediment, and redistribution on the shelf
276 during multiple dry storm events. In nature, floods and storms can coincide (wet
277 storm) or occur separately (dry storm) [e.g., 20]. Here, we set T_{flood} and T_{wave} to be
278 1250 s and 20000 s, respectively. We determine the relationship between these time
279 scales so as to satisfy a near-bypass condition on the shelf. In other words, in this

280 model framework these time scales are imposed by the relationship between the
281 sediment supply rate and wave energy.

282 The morphodynamics of the shelf generated in this scenario is shown in Fig. 4.
283 This figure shows a time series of the bed surface in the run, a feature that helps
284 describe stratigraphic architecture. Note that the interval between two lines in the
285 figure represents the deposited sediment thickness between four repeated pulse
286 inputs. At the early stage of the run, the sediment rainout from the hypopycnal
287 plume contributes the proximal sediment deposition on the bottom bed, building up
288 the shelf vertically. This shelf development is clearly recognized from the temporal
289 change of position of the rollover point. During this stage, the bed surface of the shelf
290 is well below the wave base associated with assumed wave energy, so that the
291 surface waves play no role in shelf morphodynamics. However, aggradation of the
292 shelf surface eventually results in the wave effect becoming significant. Figure 4
293 clearly shows that the rollover location starts shifting seaward when the shelf height
294 reaches 0.75 m, a point at which waves start to play a role in subaqueous sediment
295 transport. When the shelf becomes higher than wave base, the waves can entrain
296 sediment deposited on the shelf. The entrained sediment generates a weak
297 wave-supported turbidity current. This turbidity current redistributes sediment from
298 the shelf region to the slope and rise regions. As a result, the shelf elongates in the

299 seaward direction in the form of a migrating clinoform. Figure 4 suggests that shelf
300 morphodynamics at this stage is attributed to the development of a clinoform of
301 permanent form [39]. Figure 5 shows the temporal change in the slope of the slope
302 region. The continental slope becomes steeper as the shelf aggrades, but its slope
303 asymptotically reaches approximately 4° in the late stage of the simulation. This
304 behavior might be caused by sediment deposition in the rise region (i.e., build-up of
305 the basin bottom). Several mechanisms that limit the steepness of the slope such as
306 internal waves [45] and submarine groundwater flow [1] are lacking in our model, but,
307 4° is nevertheless a reasonable value for continental slopes in nature [1, 46].

308 Another interesting result of this simulation is the development of sediment
309 waves at the rollover of the modelled continental shelf. This type of morphodynamic
310 feature has been clearly observed in seismic measurements of continental margins
311 [15, 47, 48]. Figure 6 provides a more detailed view of the development of sediment
312 waves during three repeated pulse inputs. The sediment waves tend to develop
313 below the rollover, where the slope is approximately the steepest value in the
314 simulated continental slope region. These waves migrate slightly to the landward side,
315 but also disappear when they reach the shelf. As shown in Fig. 6, the wave effect
316 imposed during the entire calculation causes a bottom turbidity current (thin density
317 layer). This turbidity current plays an important role in the formation of the sediment

318 waves of Figure 6. The flow features over the sediment waves likely show the
319 presence of internal hydraulic jumps, as shown in Figs. 6b, d, and f. This upstream
320 migration of sediment waves bounded by hydraulic jumps induced by a bottom
321 turbidity current appears to be another case of deepwater mudwave cyclic steps [49].
322 The disappearance of these waves at the shelf-slope break may be due to the large
323 amount of sediment supply from hypopycnal flow, which aggrades the bed and buries
324 the waves. This aggradational tendency is much stronger near the distal end of the
325 shelf than in the slope region because the slope of the shelf surface is gentler than
326 the slope region. These effects cause repeated cycles of formation and disappearance
327 of sediment waves near the rollover of the shelf.

328 Continental shelves have most commonly been interpreted as ancient alluvial
329 or coastal plains, with sea level variation and subsequent transgression necessary for
330 their development [e.g., 3]. However, the simulation results clearly indicate that, even
331 under steady discharge and sediment supply and a stillstand condition, a self-evolving
332 continental shelf associated with seaward migrating clinoforms is possible.

333

334 **Discussion**

335 The numerical results of this study indicate that a combination of hypopycnal
336 sediment supply and wave action can lead to the formation of a continental shelf as a

337 seaward-migrating clinoform. This combination of two factors is important to the
338 formation of shelf morphology. If one of them is missing, subsequent shelf
339 morphology may be greatly different or even not realized. Hyperpycnal flows
340 contribute less to proximal sedimentation on the shelf, so that shelf sediment is less
341 available for redistributing on the clinoform by wave action than hypopycnal flows. If
342 waves are not considered, the shelf height rises to the point that it is exposed,
343 eventually resulting in a new coastal plain. However, the physical phenomena
344 described in the model are highly simplified. Below, we discuss how these
345 simplifications affect the results and interpretation, as well as the implications of the
346 numerical results for natural continental shelf formation.

347 The results indicate a purely autogenic mechanism for continental shelf
348 formation associated with seaward-migrating clinoforms driven by subaqueous
349 morphodynamic processes. While we do not say that our mechanism is the only one
350 for shelf formation, we emphasize that it needs no allogenic forcing such as sea level
351 change. Many previous studies based on sequence stratigraphy have shown that
352 allogenic effects of tectonism and sea level variation on continental shelf morphology
353 are important, and in some cases they play dominant roles in shelf genesis [3]. The
354 formation and development of continental shelves is a long-term process occurring at
355 geological timescales. Thus, long-term allogenic effects and short-term autogenic

356 processes can be expected to interact with each other. The autogenic effects analyzed
357 in this study thus may be superimposed on allogenic effects, such as the significant
358 effect of waves observed in the simulations to plane off the shelf and drive seaward
359 clinoform migration. For example, the constant sea level adopted in the simulation
360 forces vertical development of the shelf, eventually resulting in seaward clinoform
361 migration without shelf aggradation/degradation [21]. This clinoform development
362 likely leads a convex-up trajectory of the rollover point, as shown in Fig. 4. A
363 concave-up trajectory of the rollover point is also commonly observed at plate
364 margins [e.g., 3]. Sea-level variation changes wave base, so the shelf surface of this
365 model should be expected to rise or fall accordingly, as long as sediment supply is
366 commensurate to fill accommodation space so created. Sea level rise allows sustained
367 vertical development of the shelf. If waves plays a role in sediment transport at the
368 seafloor during sea level rise, the clinoform will migrate seaward. Vertical
369 development of the shelf with a migrating clinoform (i.e., sigmoid progradation [21])
370 may result in a concave up trajectory of the rollover. Such allogenic-autogenic
371 interactions need to be investigated further in the future; our results, which focus on
372 autogenic effects, can help distinguish their relative contributions to the genesis of
373 continental shelves [50].

374 Another limitation is the scale of the numerical simulation, which is here

375 performed on a small scale. We may scale up the numerical results by means of
376 Froude scale similarity, a method which has been effective for engineering-scale
377 models. Although this similarity rule cannot give in truly scale-invariant results for
378 turbidity current dynamics, the scale effect on depositional turbidity currents, i.e. the
379 weak wave-supported turbidity current associated with hypopycnal flow observed in
380 our simulations, may not be very significant [51]. However, it is useful to discuss scale
381 effects on other physical phenomena, e.g., the convection instability seen at the
382 interface between a surface sediment-laden freshwater plume and salt-rich ambient
383 water below.

384 The densimetric Froude number, F_{rd} , is defined in terms of the upstream inlet
385 conditions as follows.

$$386 \quad F_{rd} = \frac{U_{inlet}}{\sqrt{\gamma g C_{inlet} H_{inlet}}} \quad (1)$$

387 where H_{inlet} , C_{inlet} and U_{inlet} are the flow thickness, volumetric suspended sediment
388 concentration and flow velocity of inflow water at the inlet, respectively. Also g is the
389 gravitational acceleration and γ is the specific weight of sediment in water, i.e., $\gamma =$
390 $(\rho_c - \rho)/\rho$, where ρ_c and ρ are the density of sediment and water, respectively. Froude
391 similarity is satisfied when the value of F_{rd} of the model (F_{rdm}) is equal to the
392 corresponding value of the prototype (F_{rdp}) i.e., $F_{rdm} = F_{rdp}$. Note that we assume the
393 same suspended sediment concentration and specific weight of sediment between

394 the model and the prototype. This dynamic similarity then constrains the relationship
395 between the kinematic similarity parameter, λ_v , which represents the velocity ratio
396 between the model and the prototype, i.e., $\lambda_v = V_p/V_m$, and the geometric similarity
397 parameter, λ_L , which represents the length ratio between the model and the
398 prototype, i.e., $\lambda_L = L_p/L_m$, as follows.

$$399 \quad \lambda_v = \lambda_L^{1/2} \quad (2)$$

400 An appropriate length scale that characterizes continental shelves is the
401 sustained water depth on the shelf itself; we may be able to determine the geometric
402 similarity based on this water depth. In the simulation, the sustained water depth on
403 the shelf is approximately 0.2 m, yet this depth in nature is generally around 100 m.
404 This gives $\lambda_L = 500$ and $\lambda_v = 22.2$. The length scale of the numerical simulation can be
405 upscaled using this geometric similarity. The modeled clinoform relief height is
406 approximately 0.8 m, as shown in Fig. 4, resulting in an upscaled value of 400 m. This
407 is a relatively small-scale clinoform relief for the continental shelf, as seen in the New
408 Jersey margin [17], but is still larger than “platform” scale, which is a small-scale shelf
409 like morphology generally observed on a continental margin [3, 4]. It is also larger
410 than the Western Adriatic shelf clinoform [15]. The simulated height of the clinoform
411 is likely restricted by the initial depth of the basin (i.e., 1.2 m). In addition, the water
412 depth seaward of the slope increases in nature, and this has an important effect on

413 large-scale continental margin development [3]. The interplay of these limitations
414 mean that the simulated shelf formation process might specifically correspond to the
415 initial development of a continental shelf in the near-shore region.

416 In contrast to the geometric upscaling above, we now use a different sediment
417 upscaling method, that of Imran et al. [51]. First, the fall velocity in the model, v_{sm} , is
418 scaled up by means of kinematic similarity, i.e., $v_{sp} = \lambda_v v_{sm}$. The sediment diameter is
419 then back-calculated using a formula estimating the settling velocity w_f . Here, we use
420 the Stokes settling velocity for simplicity. This upscaling gives the following
421 relationships. The density flow is characterized as Froude subcritical ($F_{rd}=0.82$) at the
422 inlet, and the inlet Reynolds number, Re , is 3.7×10^7 . The upscaled sediment diameter
423 is approximately 0.1 mm, which reasonably corresponds to fine-grained suspended
424 sediment. For this size of sediment, settling-driven convection may be dominant
425 rather than double-diffusive convection, which is caused by the difference in
426 molecular diffusivity between salt and fine sediment, in forming the interfacial
427 instability beneath the hypopycnal plume [52] (see details in *SI Appendix, Methods*).
428 The upscaled wave characteristics (i.e., significant wave height of 25 m, and the wave
429 period of 22 sec) are somewhat extreme, and could exceed typical storm weather
430 conditions. However, the wave characteristics and the two time periods, which
431 represent sediment supply and wave-dominated periods (i.e., T_{flood} and T_{wave}), have

432 been chosen to achieve sediment bypass conditions on the shelf. Limited
433 computational resources constrain the computational time, so the time scales must
434 be relatively short and the wave characteristics must be extreme in the model. In
435 natural environments, the dominant wave height and period are dependent on the
436 geographic region and climate, affecting wave base and thus shelf geometry [32]. In
437 addition, the return period of the waves considered here also depends on the
438 dominant wave intensity, affecting the relation between the timescale of sediment
439 supply (depositional driver) and that of the wave-induced sediment redistribution
440 (erosional driver). This might be one of the factors causing substantial variation of
441 water depth over the continental shelves on the Earth [5]. Future development of
442 computational power will relax the model limitations described above, and will help
443 to set more reasonable computational conditions for modeling shelf
444 morphodynamics.

445 Our numerical simulations indicate that settling-driven (and double diffusive)
446 convection associated with fingering play an important role in controlling the
447 transport and fate of sediment associated with hypopycnal flows. Yet, a substantial
448 model limitation is involved in capturing the nature of this density convection. This
449 convection is a very small-scale phenomenon (*SI Appendix Methods*); thus, in
450 principle, a numerical approach suitable to capturing it would involve DNS or LES [27,

451 38, 40]. Although we capture some of the relevant convection characteristics in the
452 present model, it appears that the size of the generated plume and downward
453 density flow formed as a result is grid-dependent in the simulation. In addition to this,
454 the Reynolds-averaged approach we use here is not able to capture some of
455 important physical mechanisms of this phenomenon. For example, the turbulent
456 diffusivity modelled in Reynolds-averaged approach is generally larger than the
457 molecular diffusivity. The density convection between the surface plume and the
458 ambient water in the simulation is mainly driven by settling convection, with the
459 double diffusive effect forced to become negligibly small. Such model limitations
460 regarding the resolution of fingering is a constraint to field-scale applications of the
461 model. This is one reason why we perform our simulations in at small-scale. A
462 submodel that expresses the net sedimentation rate (or net fall velocity) from the
463 hypopycnal plume, will be essential for including this effect in large-scale models. A
464 parameter study based on a dataset obtained via DNS [41] can provide useful insight
465 in this regard. The importance of double diffusive convection (i.e., salt fingers, [56])
466 was first recognized in stratified thermohaline systems (e.g., Thermohaline Staircases)
467 [57-59]. The problem has been pursued more recently in terms of numerical
468 modeling and experiments in a sediment-salt system [27, 38, 41], so that this effect
469 will be included in large-scale models as incorporated in models of thermohaline

470 systems [e.g., 60]. But it should be realized that these fingering features are fragile,
471 and may in the field be broken up to larger-scale features by ambient turbulence. The
472 same may not be true of flocs [53, 54, 55], a model of which is difficult to implement
473 at the present model scale. Detailed field observations coupled with the numerical
474 modelling will be a significant challenge in this regard.

475 In the simulation, we neglect the alongshore dimension to simplify the
476 problem and reduce computational time. Flow and sedimentation patterns may differ
477 substantially in a three-dimensional basin. The alongshore dispersal of sediment is an
478 important factor for the behavior of positively buoyant, hypopycnal plumes [25]. This
479 lateral sediment dispersal of a hypopycnal plume associated with a river mouth (i.e.,
480 point source) greatly affects the sedimentation rate on the shelf. Neglecting the
481 lateral dimension in our simulation may overestimate the sedimentation rate on the
482 shelf. But as Cattaneo et al. [61] have shown in the Adriatic Sea (Figure 4 therein),
483 geostrophic processes can meld a line of point sources into an effective line source, to
484 which this model is applicable. Alongshore sediment dispersal is also important for
485 the flow field underneath the hypopycnal plume. For instance, Henniger and Kleiser
486 [27] performed large eddy simulations of the dynamics of hypopycnal plumes in a
487 small three-dimensional basin. They showed that, because of the limitation of the
488 model domain, a backward reverse flow (from seaward to landward) was generated.

489 Such a flow may exist in nature, but lateral dispersal of the flow will suppress this
490 flow pattern.

491 In addition to the flow field, the simulated morphodynamic features of the
492 shelf will be affected by the alongshore dimension. Sediment transport to the
493 continental slope due to the wave-induced turbidity current migrates the shelf
494 clinoform seaward, and develops sediment waves near the rollover. This result
495 suggests the formation of a strongly aggradational feature on the modeled
496 continental slope. If the alongshore dimension is considered, surface waves may force
497 a more horizontal 2D wave-supported turbidity current rather than a line-type
498 current. When such a 2D turbidity current reaches the shelf break, it may migrate the
499 clinoform, but there is also a possibility for flow focusing and the formation of
500 submarine gullies [43]. Furthermore, as mentioned in the results, a turbidity current
501 flowing along a continental slope may also causes the formation of a submarine fan
502 system [62]. These different morphodynamic processes are expected to coexist
503 during formation of a continental shelf.

504

505 **Conclusion**

506 In this study, we perform numerical simulations of continental-shelf formation. We
507 focus on two major aspects: 1) the role of saltwater in developing continental shelves,

508 and 2) self-evolving continental shelf formation with seaward-migrating clinoforms.
509 We perform our analysis with repeated pulses of water and sediment input into the
510 nearshore zone, but steady wave effects, and without allogenic effects such as sea
511 level change. There is a common understanding according to which many continental
512 shelves are essentially submerged coastal plains formed during low stand. Our results
513 suggest an additional, autogenic mechanism for continental shelf formation or
514 augmentation by purely subaqueous morphodynamic processes.

515 The first aspect of this study is intended to highlight the importance of
516 dissolved salt in ambient water on the transport and fate of terrigenous suspended
517 sediment. The numerical results clearly show different behaviors between hypo and
518 hyperpycnal flows (i.e., with and without dissolved salt in ambient water) on the
519 simulated morphodynamics of shelf morphology. Hypopycnal flow shows purely
520 depositional features in shelf development. In this flow regime, sediment-laden fresh
521 river water overlies salty ambient water in a condition of stable stratification in terms
522 of the total density of fluid. However, because of the fall velocity of sediment, an
523 interfacial instability develops between the two layers, resulting in significant
524 sediment loss from the surface hypopycnal plume. This sediment rainout
525 subsequently contributes to the development of a weak turbidity current on the
526 bottom. Such a weak current is found to be unable to entrain sediment from the

527 bottom, so that this flow condition contributes purely to proximal deposition of
528 sediment, and the formation of shelf morphology. On the contrary, hyperpycnal
529 conditions generate a relatively strong density flow on the bottom. This current may
530 cause erosion or deposition of sediment on the shelf, but most of the sediment is
531 delivered into deep water. These results indicate that dissolved salt plays an
532 important role in controlling sediment dispersal, and in suppressing direct delivery to
533 deep water.

534 The depositional features of hypopycnal flows are key for explaining the large
535 amount of sediment supply to the continental shelf. Another factor for continental
536 shelf formation is the effect of waves on the redistribution of deposited sediment on
537 the shelf. We find that, if a strong surface wave effect is imposed for a time period
538 sufficient to flush out sediment deposited by hypopycnal flows down to wave base
539 (i.e., to a bypass condition), then continental shelf development with a
540 seaward-migrating clinoform can be achieved. Wave energy resuspends sediment
541 from the bed, and the subsequent development of a wave-supported turbidity
542 current brings sediment from the shelf to the slope, where it deposits below wave
543 base. This contributes to seaward migration of the clinoform. Conversely, sediment
544 resuspension due to waves restricts further vertical accumulation of sediment on the
545 shelf, resulting in a sustained water depth on the shelf associated with the level of

546 wave base. These subaqueous hydrodynamic, sediment-transport, and
547 morphodynamic processes lead to continental shelf development with a migrating
548 clinoform, even under conditions of constant sea level.

549 In nature, autogenic subaqueous factors associated with the morphodynamics
550 of continental shelves (internal forces) are superimposed on other allogenic
551 processes, such as sea-level variation and tectonism. The relationship between
552 autogenic and allogenic effects should be clarified in future work, because sea-level
553 variation and tectonism are known to have played important roles in the formation of
554 continental shelves [3]. However, in so far as subaqueous processes have received
555 less attention in the context of continental-shelf morphodynamics, our results
556 provide new insight and interpretations of the genesis of continental shelves.

557

558 ***Methods***

559 The system modeled in this study (i.e., dynamics of hypo- and hyperpycnal
560 flows and subsequent morphodynamics of continental shelves) is complex and
561 multiscaled in both time and space. It is unreasonable to treat all the physics above in
562 a precise way using high-resolution physics-based numerical model at geological time
563 scales, so we need several simplifications (see more detail in *SI Appendix Methods*).
564 Here, we perform numerical simulations at a laboratory-scale, vertical

565 two-dimensional field (cross-shore only). The density-driven flow is calculated by an
566 unsteady Reynolds-averaged Navier-Stokes model with k - ε type turbulent closure.
567 Stratification effects on turbulence production are also considered. The transport
568 equation (advection-diffusion equation) is used to calculate the suspended sediment
569 transport and dissolved salt in the fluid. Both sediment and salt contribute to the
570 density of the fluid, whereas the temperature effect is neglected in our model. The
571 sediment is treated as a single-grain cohesionless sediment. To include the effect of
572 surface waves on sediment transport, we use a simple linear wave theory. More
573 specifically, the additional shear stress due to the presence of a wave boundary layer
574 is calculated using a linear wave theory. The details of the model and results are
575 described in SI Appendix, and the code and calculation data used in the paper can be
576 accessed at the Figshare database [63].

577

578

579 **Acknowledgement**

580 Toshiki Iwasaki and Gary Parker were supported by the ExxonMobil project “Transport,
581 Deposition and Preservation of Mud: Experimental and Numerical Approach”. We
582 acknowledge Juan Fedele, David Hoyal, Chris Paola, Juergen Schieber, Kyle Strom and
583 Andrew Wickert for discussion and insight. We thank Hajime Naruse and Andrew

584 Wickert for insightful reviews.

585

586 **References**

- 587 1. Pratson, LF, Nittrouer, CA, Wiberg, PL, Steckler, MS, Swenson, JB, Cacchione, DA,
588 Karson, JA, Murray, AB, Wolinsky, MA, Gerber, TP, Mullenbach, BL, Spinelli, GA,
589 Fulthorpe, CS, O'grady, DB, Parker, G, Driscoll, NW, Burger, RL, Paola, C, Orange, DL,
590 Field, ME, Friedrichs, CT and Fedele, JJ (2007) Seascape Evolution on Clastic
591 Continental Shelves and Slopes, in *Continental Margin Sedimentation: From
592 Sediment Transport to Sequence Stratigraphy* (eds C. A. Nittrouer, J. A. Austin, M.
593 E. Field, J. H. Kravitz, J. P. M. Syvitski and P. L. Wiberg), Blackwell Publishing Ltd.,
594 Oxford, UK. doi: 10.1002/9781444304398.ch7.
- 595 2. Carvajal, CR Steel, RJ and Petter A (2009) Sediment supply: The main driver of
596 shelf-margin growth, *Earth Sci. Rev.*, 96, 221-248.
- 597 3. Helland-Hansen, W, Steel, RJ and Somme, TO (2012) Shelf genesis revisited, *J.
598 Sediment. Res.*, 82, 133-148.
- 599 4. Patruno, S, Hampson, GJ, and Jackson, CA-L (2015) Quantitative characterization
600 of deltatic and subaqueous clinoforms, *Earth Sci. Rev.*, 142, 79-119.
- 601 5. Kennett, JP (1982) *Marine Geology*, Prentice-Hall, Englewood Cliffs, NJ, 813 pp.
- 602 6. Emery, KO (1968) Relict sediments on continental shelves of world, *Am. Assoc. Pet.*

603 *Geol. Bull.*, 52(3) 445-464.

604 7. Summerhayes, CP, Sestini, G, Misdorp, R. and Marks, N (1978) Nile delta: nature
605 and evolution of continental shelf sediments, *Mar. Geol.*, 27, 43-65.

606 8. Miller, KC, Howie, JM, and Ruppert, SD (1992) Shortening within underplated
607 oceanic crust beneath the Central California margin, *J. Geophys. Res.*, 97,
608 19961-19980.

609 9. Weight, RWR, Anderson, JB and Fernandez, R (2011) Rapid mud accumulation on
610 the central Texas shelf linked to climate change and sea-level rise, *J. Sediment Res.*,
611 81, 743-764.

612 10. Palinkas, CM and Nittrouer, CA (2004) Clinoform sedimentation along the
613 Apennine shelf, Adriatic Sea, *Mar. Geol.*, 234, 245-260.

614 11. Niedoroda, AW, Reed CW, Das, H, Fagherazzi, S, JDonoghue, JF and Cattaneo, A
615 (2005) Analyses of a large-scale depositional clinoformal wedge along the Italian
616 Adriatic coast, *Mar. Geol.*, 222-223, 179-192.

617 12. Aller, RC, Heilbrun, C, Panzeca, C, Zhu, Z-B and Baltzer, F (2004) Coupling between
618 sedimentary dynamics, early diagenetic processes, and biogeochemical cycling in
619 the Amazon-Guianas mobile mud belt: coastal French Guiana, *Mar. Geol.*, 208,
620 331-360.

621 13. Yang, G-S and Liu, J-P (2007) A unique Yellow River-derived distal subaqueous

- 622 delta in the Yellow Sea, *Mar. Geol.*, 240, 169–176.
- 623 14. Gao, S. and Collins, MB (2014) Holocene sedimentary systems on continental
624 shelves, *Mar. Geol.*, 352, 268–294.
- 625 15. Cattaneo, A, Trincardi, F, Asioli, A and Correggiari, A (2007) The Western Adriatic
626 shelf clinoform: energy-limited bottomset, *Cont. Shelf Res.*, 27, 506-525.
- 627 16. Maselli, V, Hutton, EW, Kettner, AJ, Syvitski, JPM and Trincardi, F (2011)
628 High-frequency sea level and sediment supply fluctuations during Termination I:
629 An integrated sequence-stratigraphy and modeling approach from the Adriatic
630 Sea (Central Mediterranean), *Mar. Geol.*, 287, 54-70.
- 631 17. Steckler, MS, Moutain, GS, Miller, KG and Christie-Blick, N (1999) Reconstruction
632 of Tertiary progradation and clinoform development on the New Jersey passive
633 margin by 2-D backstripping, *Mar. Geol.*, 154, 399-420.
- 634 18. Carter, L and Heath, RA (1975) Role of mean circulation, tides, and waves in the
635 transport of bottom sediment on the New Zealand continental shelf, *N. Z. J. Mar.*
636 *Freshwater Res.*, 9(4), 423-448.
- 637 19. Harris, CK, Traykovski, PA and Geyer, WR (2005) Flood dispersal and deposition by
638 near-bed gravitational sediment flows and oceanographic transport: A numerical
639 modeling study of the Eel River shelf, northern California, *J. Geophys. Res.*, 110,
640 C09025, doi:10.1029/2004JC002727.

- 641 20. Traykovski, P, Wiberg, PL and Geyer, WR (2007) Observations and modeling of
642 wave-supported sediment gravity flows on the Po prodelta and comparison to
643 prior observations from the Eel shelf, *Cont. Shelf Res.*, 27, 375-399.
- 644 21. Catuneanu, O, Abreu, V, Bhattacharya, JP, Blum, MD, Dalrymple, RW, Eriksson, PG,
645 Fielding, CR, Fisher, WL, Galloway, WE, Gibling, MR, Giles, KA, Holbrook, JM,
646 Jordan, R, Kendall, CG StC, Macurda, B, Martinsen, OJ, Miall, AD, Neal, JE,
647 Nummedal, D, Pomer, L, Posamentier, HW, Pratt, BR, Sarg, JF, Shanley, KW, Steel,
648 RJ, Strasser, A, Tucker, ME, and Winker, C (2009) Towards the standardization of
649 sequence stratigraphy, *Earth Sci. Rev.*, 92, 1-33.
- 650 22. Muto, T, Steel, RJ and Swenson, JB (2007) Autostratigraphy: A framework norm for
651 genetic stratigraphy, *J. Sediment. Res.*, 77, 2-12.
- 652 23. Mulder, T and Syvitski, JPM (1995) Turbidity currents generated at river mouths
653 during exceptional discharges to the world oceans, *J. Geol.*, 103, 285-299.
- 654 24. Wang, HJ, Yang, ZS, Saito, Y, Liu, JP and Sun, X (2006) Interannual and seasonal
655 variation of the Huanghe (Yellow River) water discharge over the past 50 years:
656 Connections to impacts from ENSO events and dams, *Glob. Planet. Change*, 50,
657 212-225.
- 658 25. Horner-Devine, A, Hetland, R and MacDonald, D (2015) Mixing and transport in
659 coastal river plumes, *Annu. Rev. Fluid Mech.*, 47, 569-594.

- 660 26. McCool, WW, and Parsons, JD (2004) Sedimentation from buoyant fine-grained
661 suspensions, *Cont. Shelf Res.*, 24, 1129-1142.
- 662 27. Henniger, R, Kleiser, L and Meiburg, E (2010) Direct numerical simulations of
663 particle transport in a model estuary, *J. Turbul.*, 11, N39, doi:
664 10.1080/14685248.2010.516257.
- 665 28. Sherstyankin, PP, Alekseev, P, Abramov, AM, Stavrov, KG, De Batist, M, Canals, M,
666 and Casamor, JL (2006) Computer-based bathymetric map of Lake Baikal, *Dokl.*
667 *Earth Sci.*, 408(1), 564-569.
- 668 29. Nutz, A, Schuster, M, Ghienne, JF, Roquin, C, Hay, MB, Retif, F, Certain, R, Robin, N,
669 Raynal, O, Cousineau, PA, SIROCCO team, and Bouchette, F (2015) Wind-driven
670 bottom currents and related sedimentary bodies in Lake Saint-Jean (Quebec,
671 Canada), *Geol. Soc. Am. Bull.*, 127:9-10, 1194-1208.
- 672 30. Fenneman, NM (1902) Development of the profile of equilibrium of the
673 subaqueous shore terrace, *J. Geol.*, 10, 1-32.
- 674 31. Johnson, DW (1919) Shore processes and shoreline development, John Wiley &
675 Sons, New York, 584 p.
- 676 32. Sunamura, T (1978) A model of the development of continental shelves having
677 erosional origin, *Geol. Soc. Am. Bull.*, 89, 504-510.
- 678 33. Higgs, R (2010) Why do siliciclastic shelves exist? How do they differ from "Ramp

- 679 margins"? New sequence stratigraphic aspects vital for petroleum exploration,
680 *AAPG Search and Discovery Article #40527*, 12 p.
- 681 34. Yoshikawa, T (1997) Continental shelves: their origin, Kokon-shoten, 202 pp.
- 682 35. Dietz, R and Menard, H (1951) Origin of abrupt change in slope at continental
683 shelf margin, *AAPG bulletin*, 35, 1994-2016.
- 684 36. Friedrichs, CT and Wright, LD (2004) Gravity-driven sediment transport on the
685 continental shelf: implications for equilibrium profiles near river mouths, *Coast.*
686 *Eng.*, 51, 795-811.
- 687 37. Maxworthy, T (1999) The dynamics of sedimenting surface gravity currents, *J.*
688 *Fluid Mech.*, 392, 27-44.
- 689 38. Henniger, R and Kleiser, L (2012) Temporal evolution, morphology, and settling of
690 the sediment plume in a model estuary, *Phys. Fluids*, 24, 086601,
691 doi:10.1063/1.4739537.
- 692 39. Parker, G (2006) Theory for a clinoform of permanent form on a continental
693 margin emplaced by weak, dilute muddy turbidity currents, Proceedings of the
694 4th IAHR Symposium on River, Coastal and Estuarine Morphodynamics,
695 RCEM2005 –Urbana, IL, United States, 553-561.
- 696 40. Burns, P and Meiburg, E (2012) Sediment-laden fresh water above salt water:
697 linear stability analysis, *J. Fluid Mech.*, 691, 279-314.

- 698 41. Burns, P and Meiburg, E (2015) Sediment-laden fresh water above salt water:
699 nonlinear simulations, *J. Fluid Mech.*, 762, 156-195.
- 700 42. Syvitski, JPM, Asprey, KW, Clattenberg, DA, and Hodge, GD (1985) The prodelta
701 environment of a fjord: Suspended particle dynamics, *Sedimentology*, 32, 83-107.
- 702 43. Parsons, JD, Bush, JWM, and Syvitski, JPM (2001) Hyperpycnal plume formation
703 from riverine outflows with small sediment concentrations, *Sedimentology*, 48,
704 465-478.
- 705 44. Izumi, N (2004) The formation of submarine gullies by turbidity currents, *J.*
706 *Geophys. Res. Oceans*, 109, C03048, doi:10.1029/2003JC001898.
- 707 45. Ribo, M, Puig, P, Munoz, A, Iacono, CL, Masque, P, Palangues, A, Acosta, J, Guillen,
708 J and Ballesteros, MG (2016) Morphobathymetric analysis of the large
709 fine-grained sediment waves over the Gulf of Valencia continental slope (NW
710 Mediterranean), *Geomorphology*, 253, 22-37.
- 711 46. O'Grady, DB, Syvitski, JPM, Pratson, LF and Sarg, JF (2000) Categorizing the
712 morphologic variability of siliciclastic passive continental margins, *Geology*, 28,
713 207-210.
- 714 47. Wynn, RB, Masson, DG, Stow, DAV and Weaver, PPE (2000) Turbidity current
715 sediment waves on the submarine slopes of the western Canary Islands, *Mar.*
716 *Geol.*, 163(1-4), 185-198.

- 717 48. Lee, HJ, Syvitski, JPM, Parker, G, Orange, D, Locat, J, Hutton, EWH and Imran, J
718 (2002) Distinguishing sediment waves from slope failure deposits: field examples,
719 including the “Humboldt Slide”, and modelling results. *Mar. Geol.*, 192, 79–104.
- 720 49. Kostic, S, Sequeiros O, Spinewine, B and Parker, G (2010) Cyclic steps: A
721 phenomenon of supercritical shallow flow from the high mountains to the bottom
722 of the ocean, *J. Hydro Environ. Res.*, 3(4), 167-172.
- 723 50. Yang, W, Kominz, MA and Major, RP (1998) Distinguishing the roles of autogenic
724 versus allogenic processes in cyclic sedimentation, Cisco Group (Virgilian and
725 Wolfcampian), north-central Texas, *Geol. Soc. Am. Bull.*, 110(10), 1333-1353.
- 726 51. Imran, J, Khan, SM, Pirmez, C and Parker, G (2017) Froude scaling limitations in
727 modeling of turbidity currents, *Environ. Fluid Mech.*, 17, 159-186.
- 728 52. Yu, X, Hsu, T-J and Balachandar, S (2013) Convective instability in sedimentation:
729 Linear stability analysis, *J. Geophys. Res. Oceans*, 118, 256–272,
730 doi:10.1029/2012JC008255.
- 731 53. Syvitski, JPM, Asprey, KW and Leblanc, KWG (1995) In-situ characteristics of
732 particles settling within a deep-water estuary, *Deep Sea Res. II*, 42, 223-256.
- 733 54. Winterwerp, JC (1998) A simple model for turbulence induced flocculation of
734 cohesive sediment, *J. Hydraul. Res.*, 36:3, 309-326.
- 735 55. Maerz, J, Verney, R, Wirtz, K and Feudel, U (2011) Modeling flocculation

- 736 processes: Intercomparison of a size class-based model and a distribution-based
737 model, *Cont. Shelf Res.*, 31, S84-S93.
- 738 56. Stern, M (1969) Collective instability of salt fingers, *J. Fluid Mech.*, 35(2), 209-218.
- 739 57. Schmitt, RW (1994) Double diffusion in oceanography, *Annu. Rev. Fluid Mech.*, 26,
740 255-285.
- 741 58. Merryfield, WJ (1999) Origin of thermohaline staircases, *J. Phys. Oceanogr.*, 30,
742 1046-1068.
- 743 59. Schmitt, RW, Ledwell, JR, Montgomery, ET, Polzin, KL and Toole, JM (2005)
744 Enhanced diapycnal mixing by salt fingers in the thermocline of the tropical
745 Atlantic, *Science*, 308, 685-688.
- 746 60. Zhang, J, Schmitt, RW and Huang, RX (1998) Sensitivity of the GFDL modular
747 ocean model to parameterization of double-diffusive processes, *J. Phys.*
748 *Oceanogr.*, 28, 589-605.
- 749 61. Cattaneo, A, Correggiari, A, Langone, L and Trincardi, F (2003) The late-Holocene
750 Gargano subaqueous delta, Adriatic shelf: Sediment pathways and supply
751 fluctuations, *Mar. Geol.*, 193, 61-91.
- 752 62. Covault, JA (2011) Submarine Fans and Canyon-Channel Systems: A Review of
753 Processes, Products, and Models. *Nature Education Knowledge*, 3(10):4
- 754 63. Iwasaki, T. and Parker, G (2019) Code and calculation data for the subaqueous

755 formation process of continental shelves. Figshare.

756 <https://doi.org/10.6084/m9.figshare.10295450>. Deposited 13 November 2019.

757

758 **Figure Captions**

759 Figure 1. Simulation results of hypopycnal flow in Case 1: a) suspended sediment
760 transport expressed by the excess density due to sediment; b) dissolved salt transport
761 expressed by the excess density due to salt; and c) magnitude of flow velocity.

762 Figure 2. Simulation results of hyperpycnal flow in Case 1: a) suspended sediment
763 transport expressed as excess density due to sediment; and b) magnitude of flow
764 velocity.

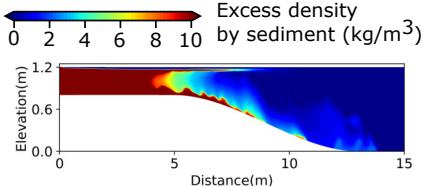
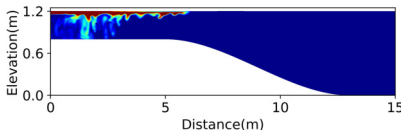
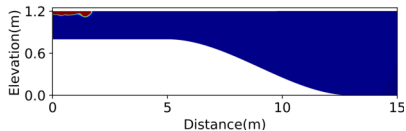
765 Figure 3. Bed surface profiles developed by the hypo- and hyperpycnal flows of Case 1
766 (see *SI Table-S1*) after 4 hours of simulation.

767 Figure 4. Computational result of shelf morphology development without an initial
768 proto-shelf. The time interval between each line represents the time between four
769 repeated pulse inputs, i.e., $4(T_{\text{flood}} + T_{\text{wave}})$. The blue points denote the rollover point,
770 which is determined by the maximum curvature of shelf morphology, and the solid
771 black line shows the time change of position of the rollover points.

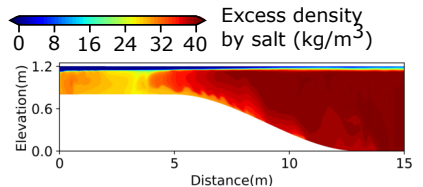
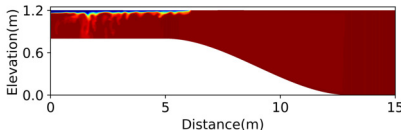
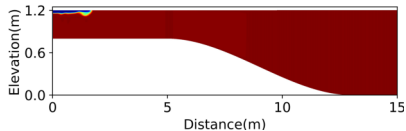
772 Figure 5. Temporal change in modelled continental slope steepness corresponding to
773 the case of Figure 4.

774 Figure 6. Development of sediment waves at the shelf rollover through three
775 repeated pulse inputs.

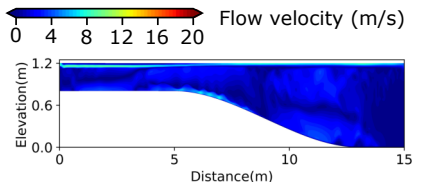
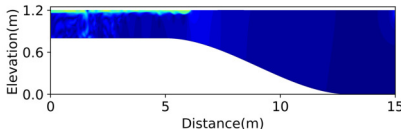
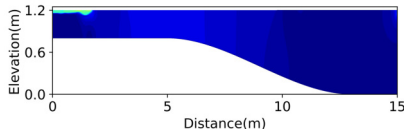
a) Suspended sediment transport



b) Dissolved salt transport



c) Hydrodynamics

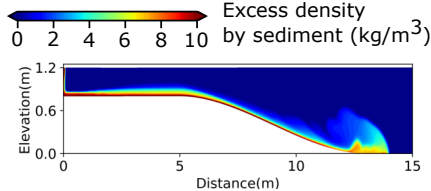
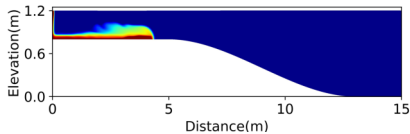
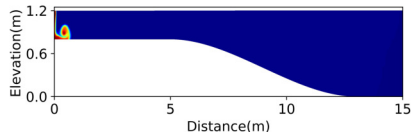


1) Time = 20 s

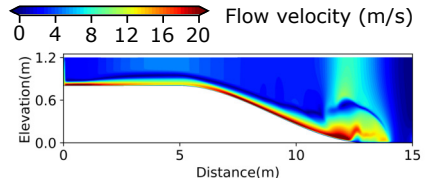
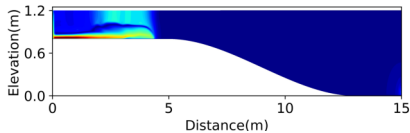
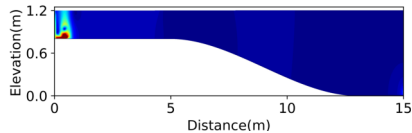
2) Time = 70 s

3) Time = 490 s

a) Suspended sediment transport



b) Hydrodynamics



1) Time = 10 s

2) Time = 50 s

3) Time = 140 s

